



兰州大学

LANZHOU
UNIVERSITY

自强不息 独树一帜

天然缪子成像技术在文物保护与矿藏勘探中的应用

Application of Muography in Conservation of Cultural Relics and Exploration of Mineral Deposits

Kaiqiang Yao

School of Nuclear Science and Technology, Lanzhou University
Frontier Science Center for Rare Isotopes, Lanzhou University
VMI China/Global

April 21, 2024



Outline

01 / Introduction

02 / Muography System

03 / Cultural relics protection-Xi'an defensive walls

04 / Mineral Exploration-Zaozigou gold mine

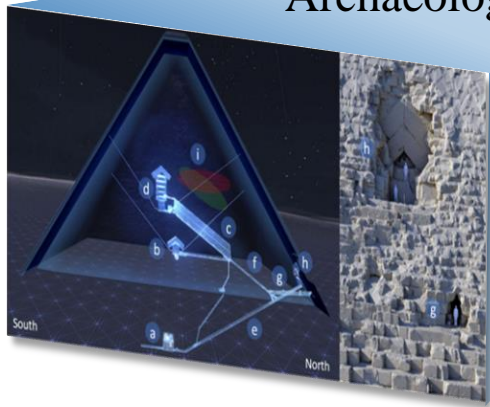
05 / Summary and Prospect

1.1 Research background

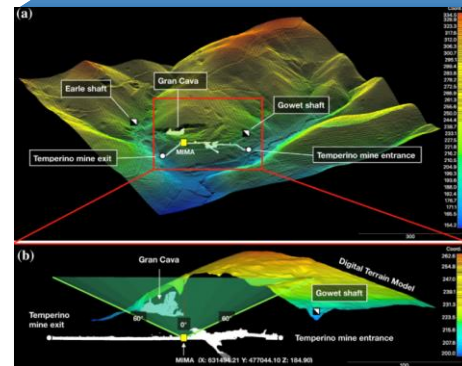
Muography is a new **green nuclear technology** that has been rapidly developed in recent years. It is widely used in materials identification, spent fuel container safety monitoring, ironmaking blast furnace imaging, internal structure monitoring of volcanoes, mineral exploration, archaeology, glacier surveying, nuclear reactor structure monitoring and so on.

Muography

Archaeology



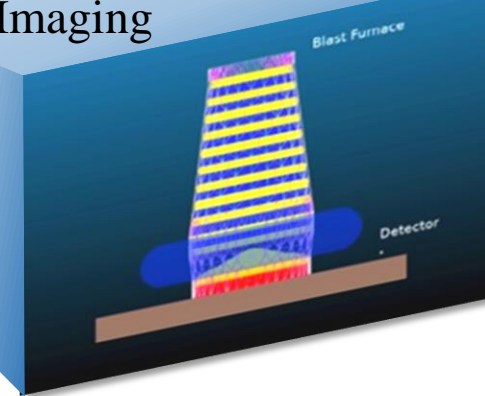
Mineral Exploration



Reactor Imaging

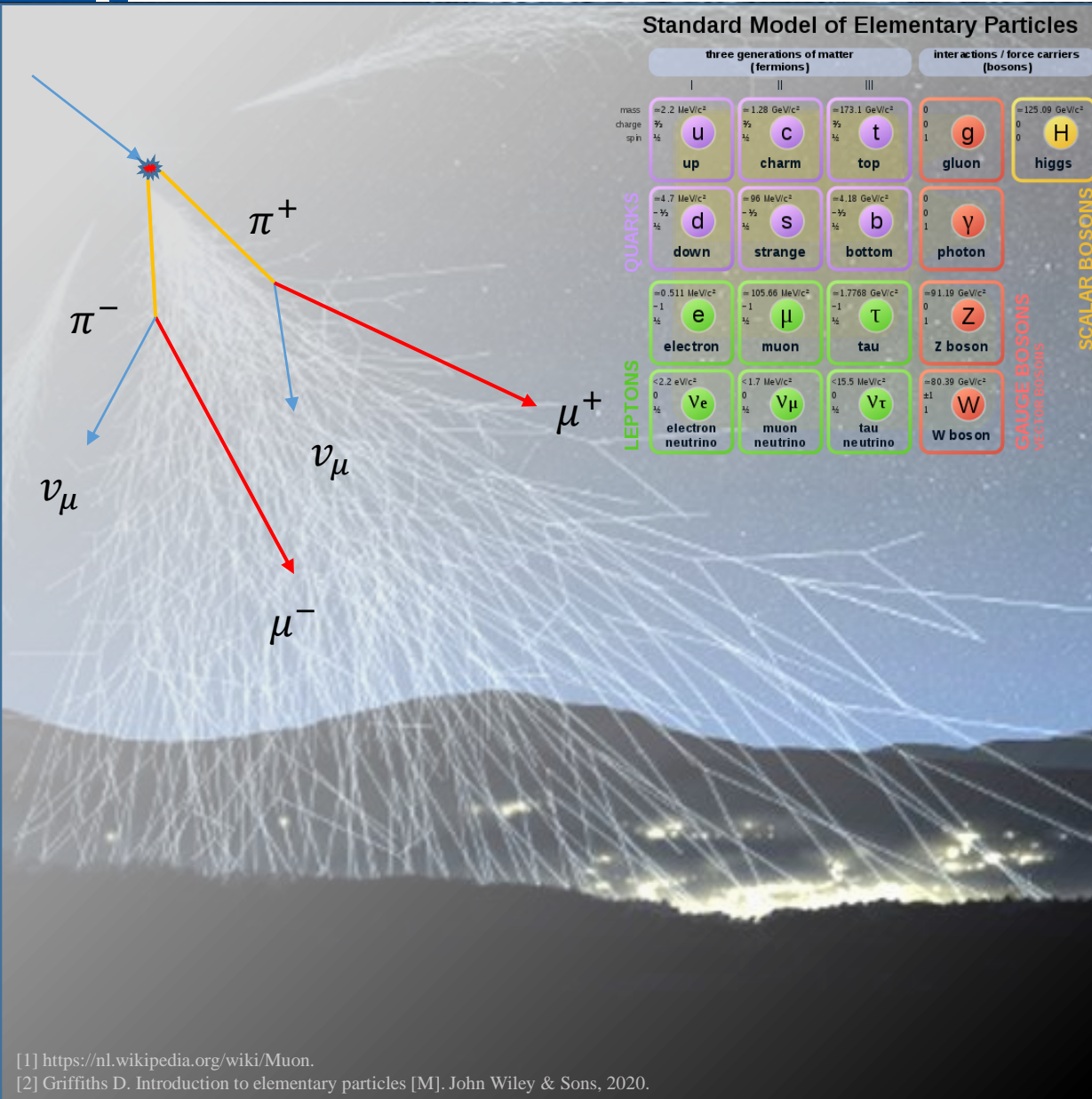


Blast Furnace Imaging



- [1] Procureur S, Morishima K, Kuno M, et al. Precise characterization of a corridor-shaped structure in Khufu's Pyramid by observation of cosmic-ray muons[J]. Nature Communications, 2023, 14(1): 1144.
- [2] Beni T, Borselli D, Bonechi L, et al. Transmission-Based Muography for Ore Bodies Prospecting: A Case Study from a Skarn Complex in Italy[J]. Natural Resources Research, 2023: 1-19.
- [3] Procureur S, Attié D, Gallego L, et al. 3D imaging of a nuclear reactor using muography measurements[J]. Science Advances, 2023, 9(5): eabq8431.
- [4] Lorenzon A, Andretto P, Checchia P, et al. Application of Muon Radiography to Blast Furnaces: the BLEMAB project[J]. La Metallurgia Italiana, 2022 (10): 62-68.

1.2 Cosmic ray muon



Cosmic ray muon production:

$$\pi^\pm \rightarrow \mu^\pm + \nu_\mu (\bar{\nu}_\mu)$$

$$K^\pm \rightarrow \mu^\pm + \nu_\mu (\bar{\nu}_\mu)$$

1

Production:
 □ Secondary particles produced by the cascade reaction of high-energy primary cosmic rays (mainly protons) with the atmosphere

2

Sea level energy and fluxes:
 □ The average energy is 4 GeV, 1 muon per square centimeter per minute.

3

Solid angle distribution:
 □ $\cos^n \theta$, $n \approx 2$ Changes with energy, elevation, latitude

4

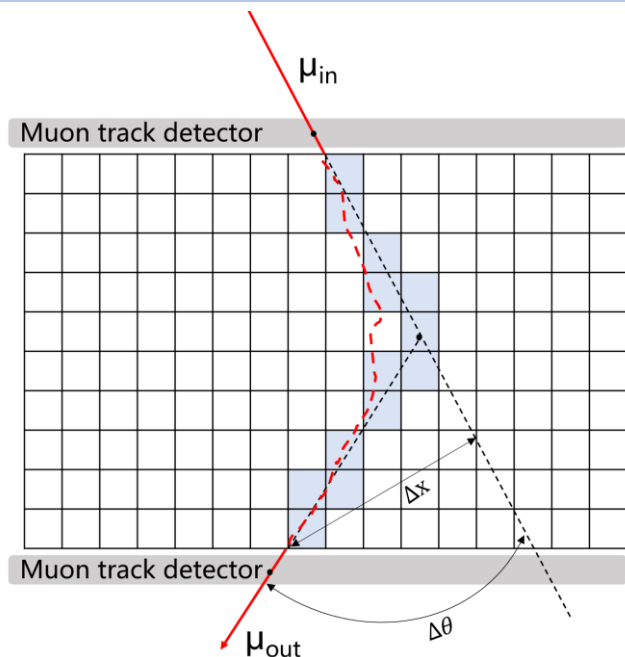
Flux influences:
 □ Fluxes are correlated with solar activity cycles, temperature, barometric pressure, altitude, latitude, and other factors

[1] <https://nl.wikipedia.org/wiki/Muon>.

[2] Griffiths D. Introduction to elementary particles [M]. John Wiley & Sons, 2020.

1.3 Principle of Muography

Based on the angular scattering principle



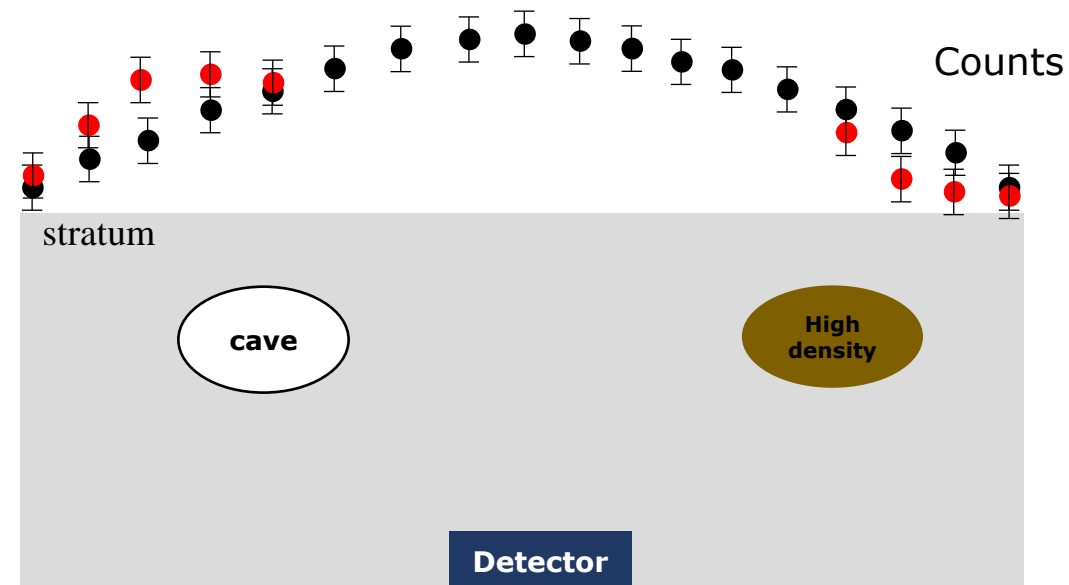
Root mean square of scattering angle

$$\sigma_{\theta} = \frac{13.6 \text{ MeV}}{\beta c p} \sqrt{\frac{L}{L_{\text{rad}}}} \left[1 + 0.038 \ln\left(\frac{L}{L_{\text{rad}}}\right) \right]$$

Radiation length

$$\frac{1}{L_{\text{rad}}} \propto \frac{Z(Z+1)}{A} \ln\left(\frac{287}{\sqrt{Z}}\right)$$

Based on the transmission principle



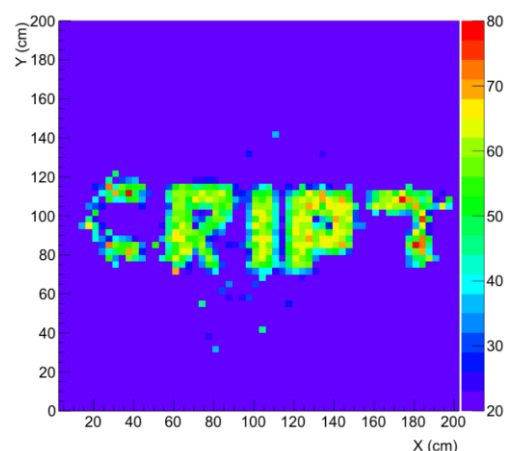
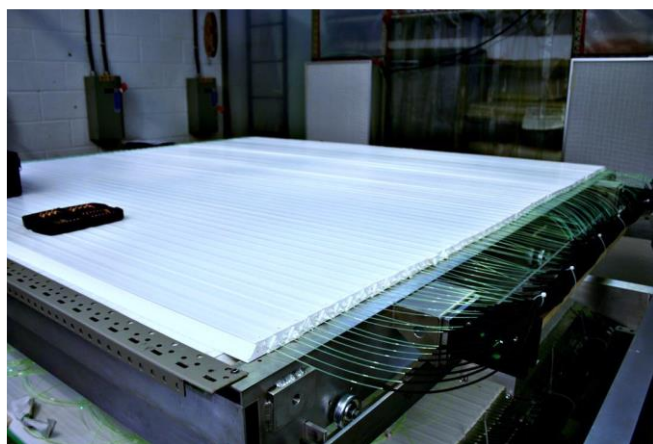
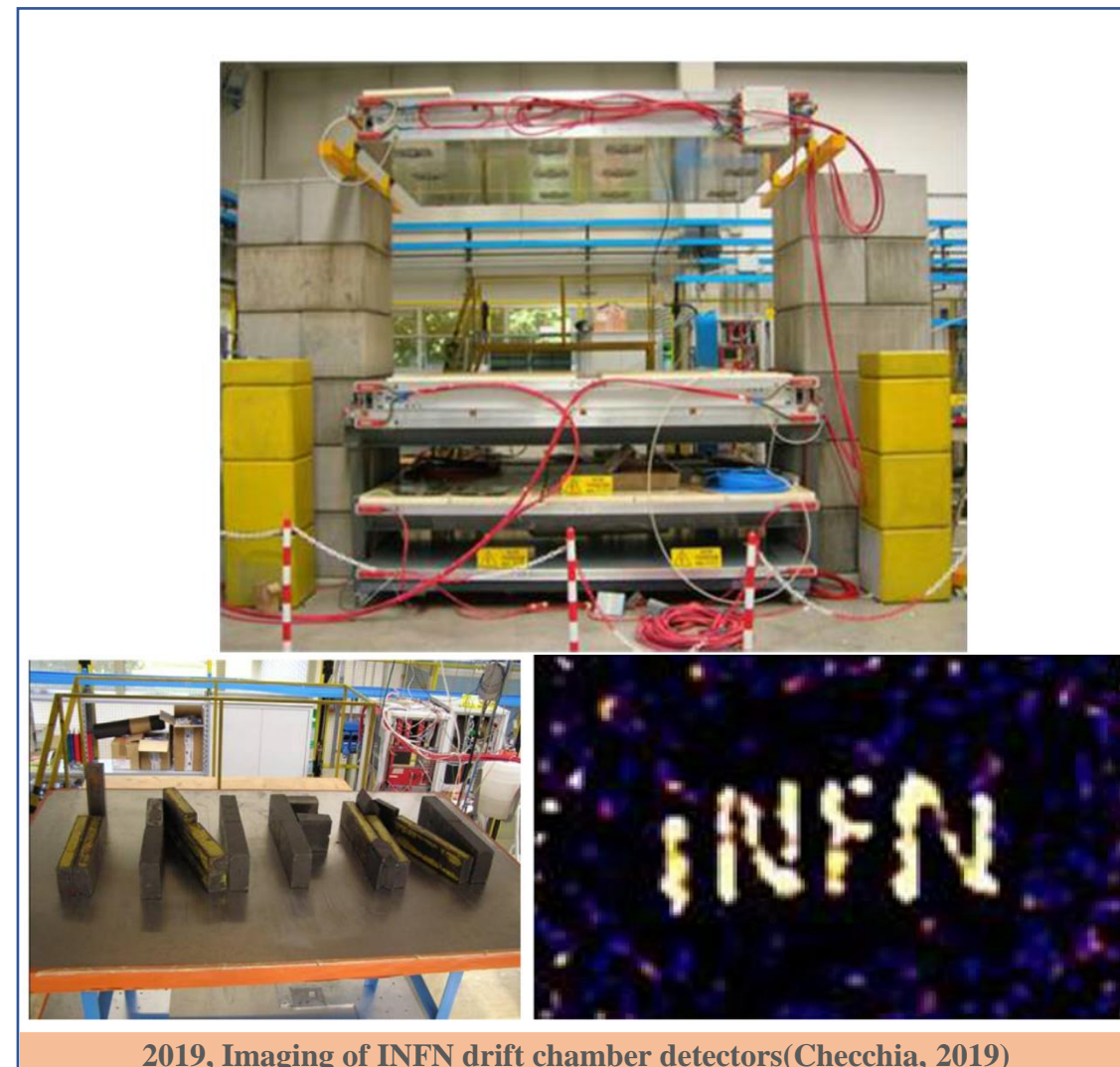
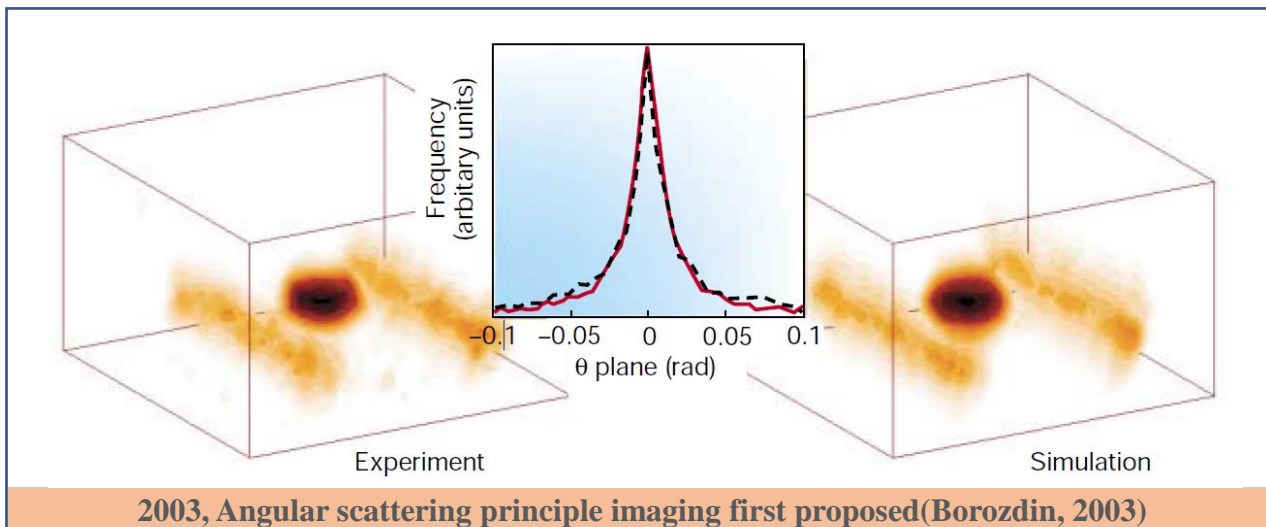
$$E_{\mu} < 500 \text{ GeV}$$

Ionization losses dominate

Bethe-Bloch equation

$$-\frac{dE}{dX} = K Z^2 \frac{1}{\beta^2} \left[\frac{1}{2} \ln \frac{2m_e c^2 \beta^2 \gamma^2 W_{\text{max}}}{I^2} - \beta^2 - \frac{\delta(\beta\gamma)}{2} \right]$$

1.4 Application of Muography



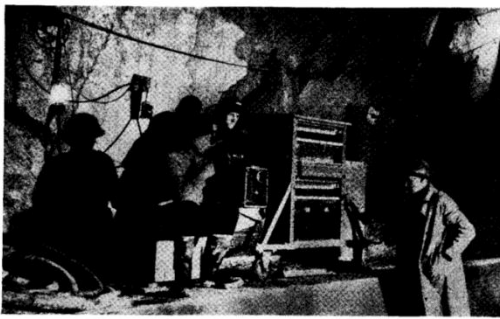
2015, Imaging of lead bricks with the TRIUMF system(Anghel, 2015)

[1] Borozdin K N, Hogan G E, Morris C, et al. Radiographic imaging with cosmic-ray muons[J]. Nature, 2003, 422(6929): 277.
[2] Anghel V, Armitage J, Baig F, et al. A plastic scintillator-based muon tomography system with an integrated muon spectrometer[J]. NIMA, 2015, 798: 12-23.
[3] Cecchia P, Benettoni M, Bettella G, et al. INFN muon tomography demonstrator: past and recent results with an eye to near-future activities[J]. Philosophical Transactions of the Royal Society A, 2019, 377(2137): 20180065..

1.4 Application of Muography

Commonwealth Engineer, July 1, 1955 455

Cosmic Rays Measure Overburden of Tunnel

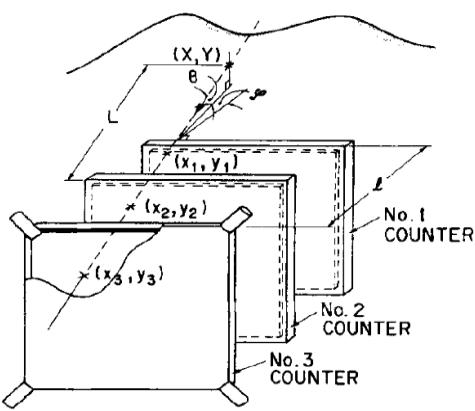


● Fig. 1—Geiger counter "telescope" in operation in the Guthega-Munyang tunnel. From left are Dr. George and his assistants, Mr. Lehane and Mr. O'Neill.

Geiger counter telescope used for mass determination at Guthega project of Snowy Scheme . . . Equipment described

By Dr. E. P. George
University of Sydney, N.S.W.

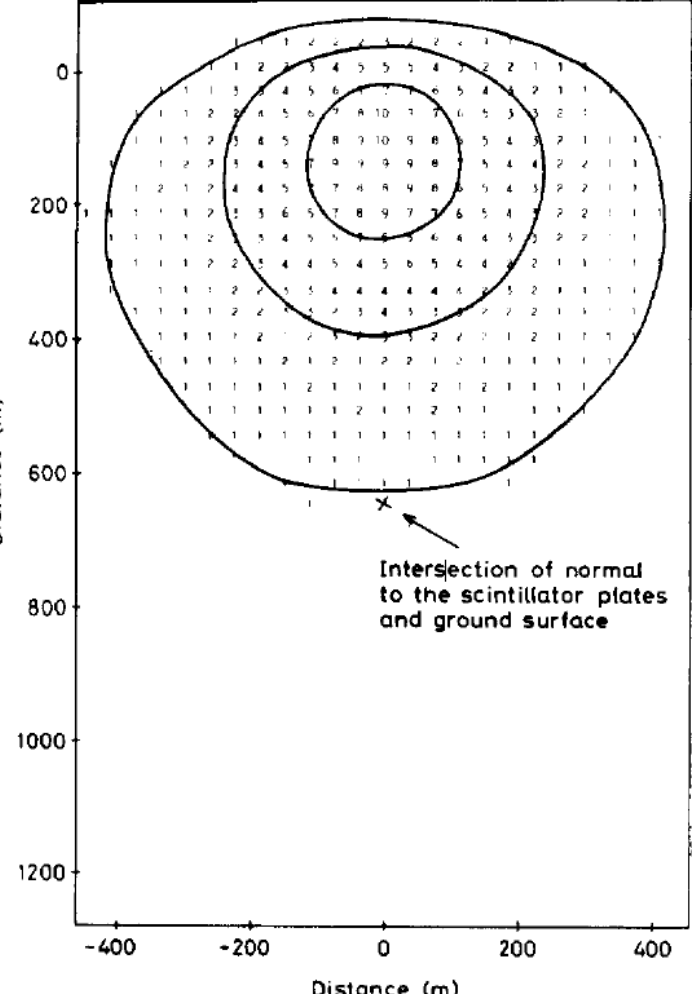
1955, First application of muon detection(George)



1995, First application of muon volcano detection(Nagamine)



1970, First archaeological exploration Alvarez)



1979, First proof of principle of muon prospecting(Malmqvist)

[1] George, E. P. (1955). Cosmic rays measure overburden of tunnel. Commonwealth Engineer, 455.
 [2] Alvarez L W, Anderson J A, Bedwei F E, et al. Search for Hidden Chambers in the Pyramids: The structure of the Second Pyramid of Giza is determined by cosmic-ray absorption[J]. Science, 1970, 167(3919): 832-839.
 [3] Malmqvist L, Jönsson G, Kristiansson K, et al. Theoretical studies of in-situ rock density determinations using underground cosmic-ray muon intensity measurements with application in mining geophysics [J]. Geophysics, 1979, 44(9): 1549-69.
 [4] Nagamine, K., Iwasaki, M., Shimomura, K., & Ishida, K. (1995). Method of probing inner-structure of geophysical substance with the horizontal cosmic-ray muons and possible application to volcanic eruption prediction. NIMA, 356(2-3), 585-595.



Outline

01 / Introduction

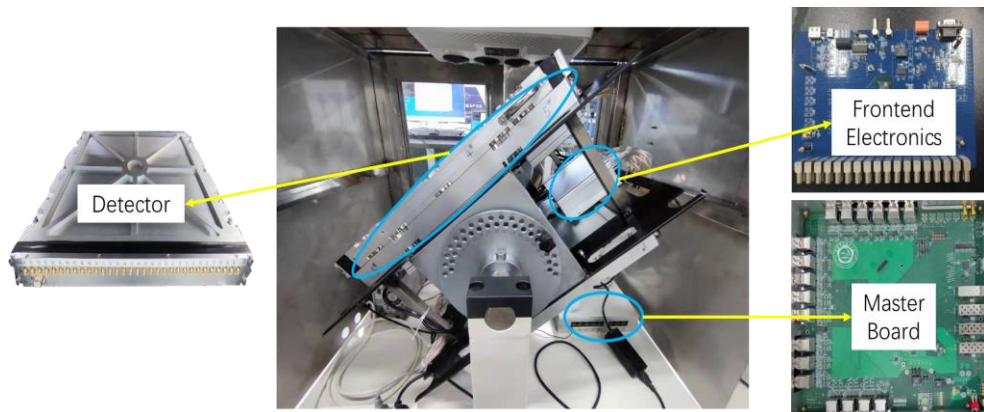
02 / Muography System

03 / Cultural relics protection-Xi'an defensive walls

04 / Mineral Exploration-Zaozigou gold mine

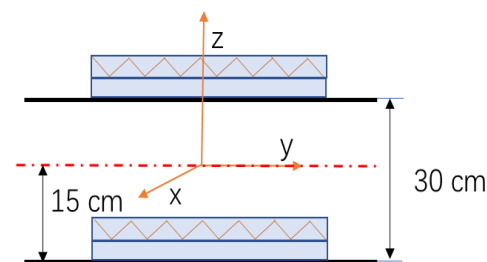
05 / Summary and Prospect

2.1 CORMIS(Cosmic Ray Muon Imaging System)

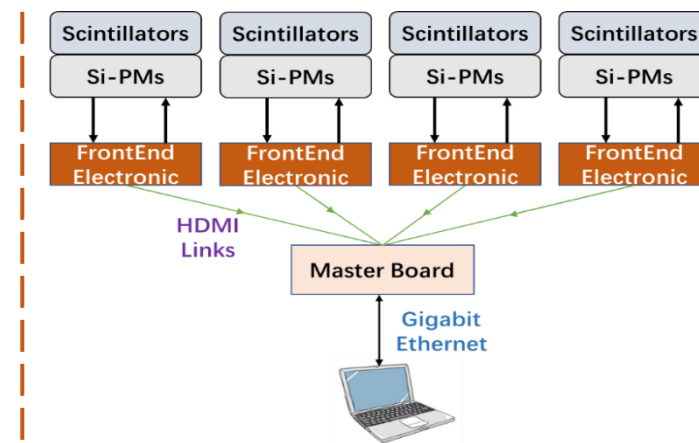


Detector Layers 0-1

Detector Layers 2-3



CORMIS internal structure



connection schematic



CORMIS (COsmic Ray Muon Imaging System) component:

- ◆ 4 layer detectors
- ◆ Acquisition system
- ◆ Remote monitoring and control platform

System Stability

Damp proof

Anti-vibration

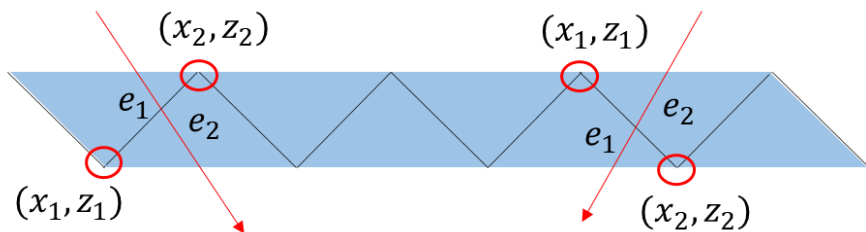
Temperature control

Angle adjustment

2.2 Plastic Scintillator Detector

2D position calculation

Arrangement

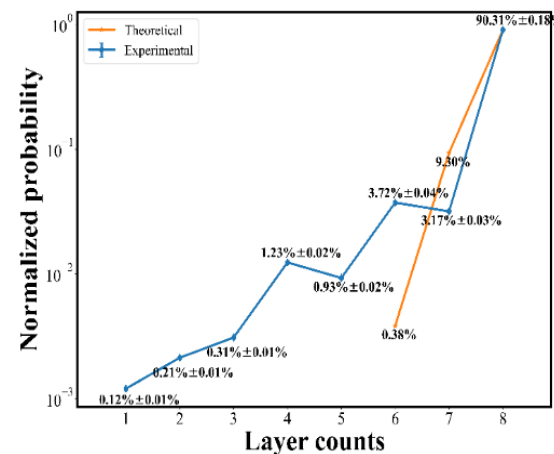


Equation

$$x = \frac{x_1 * e_1 + x_2 * e_2}{e_1 + e_2}$$

$$z = \frac{z_1 * e_1 + z_2 * e_2}{e_1 + e_2}$$

Detector efficiency

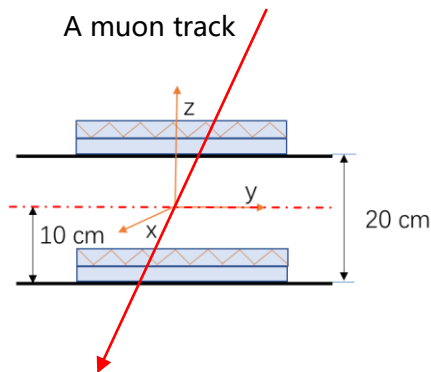


Detection efficiency of single-layer : ~97.98%

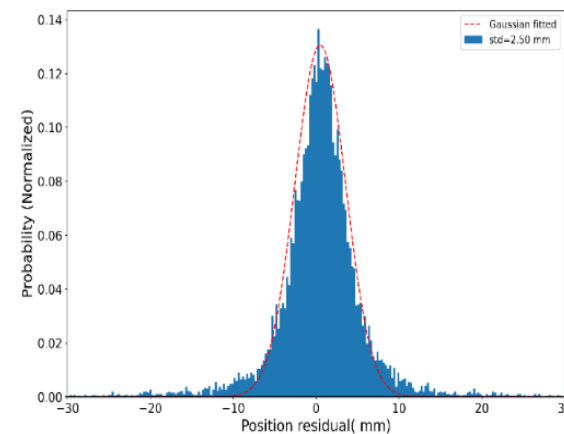
3D track calculation

Detector Layers 0-1

Detector Layers 2-3

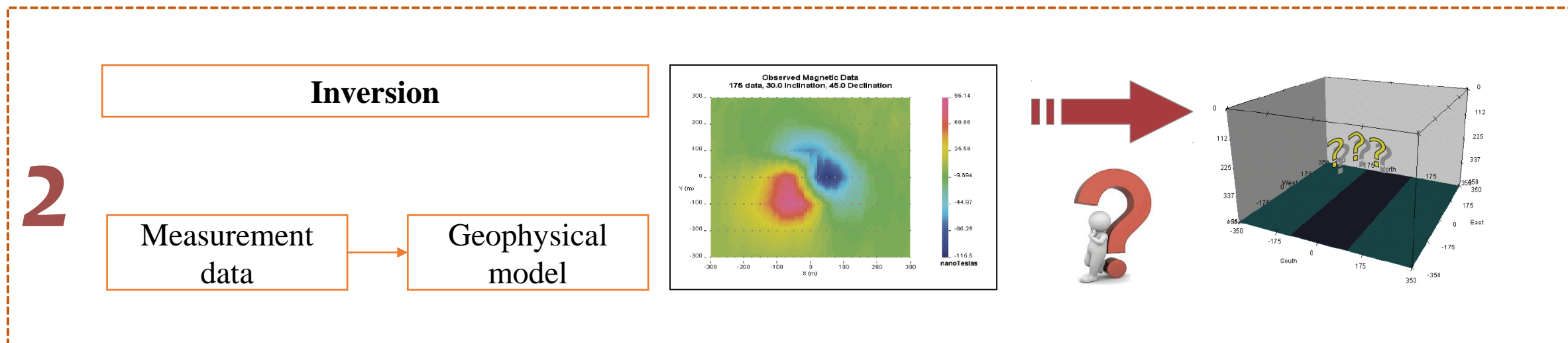
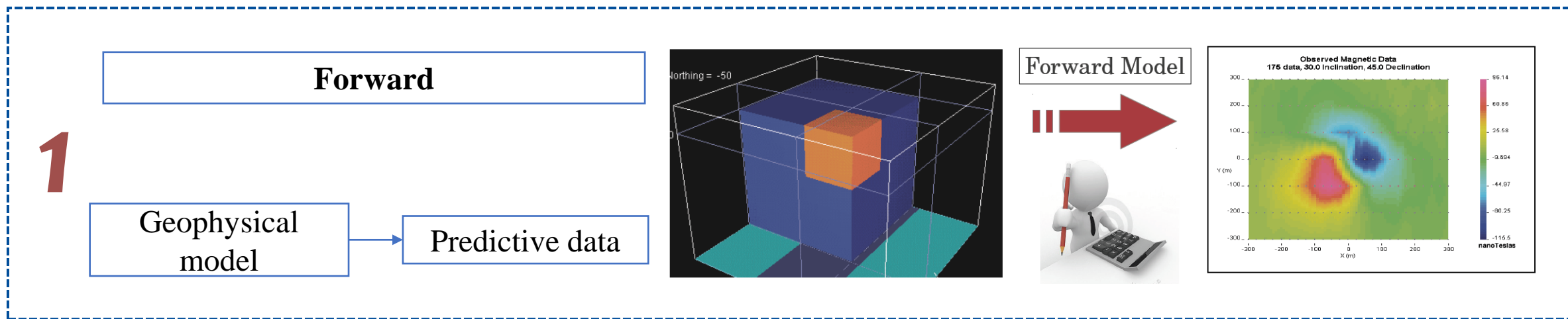


Positional resolution



Std = 2.50 mm

2.3 Forward and Inversion



2.3 Forward and Inversion

Relation among variables:

$$L_{\text{eff}} \xleftrightarrow{-\frac{dE}{dl} = a(E) + b(E)E} E_{\text{min}}(L_{\text{eff}}) \xleftrightarrow{R = \frac{\int_{E_{\text{min}}}^{\infty} \Phi(E, \theta) dE}{\int_{E_0}^{\infty} \Phi(E, \theta) dE}} R(\theta, L)$$

Measured survival rate :

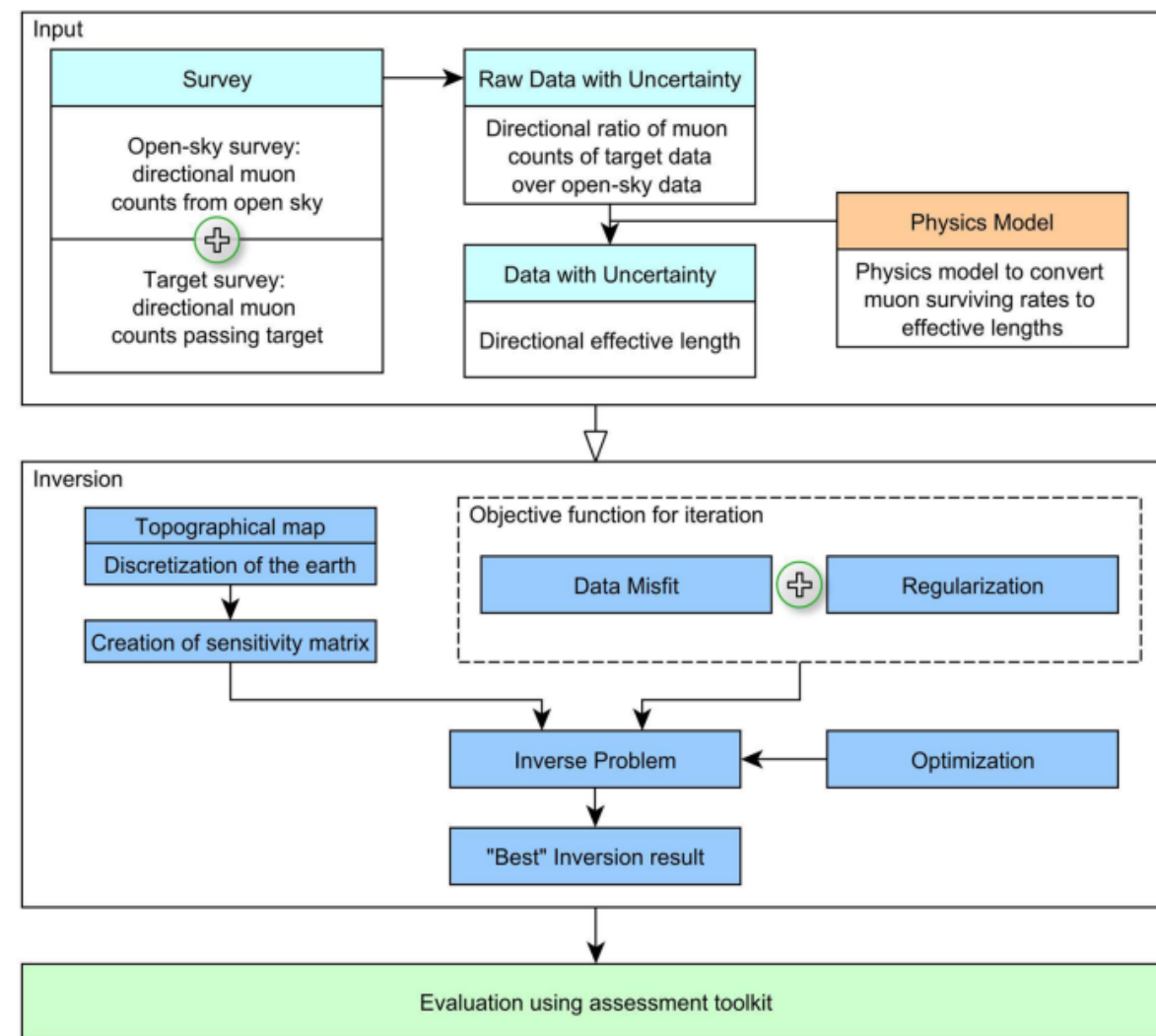
$$R^{\text{exp}}(\theta, \varphi) = \frac{N_{\text{out}}(\theta, \varphi) / \Delta T_{\text{out}}}{N_{\text{in}}(\theta, \varphi) / \Delta T_{\text{in}}}$$

Effective length:

$$L_{\text{eff}}(\theta, \varphi) = \int_{(\theta, \varphi)} \rho(x, y, z) dl$$

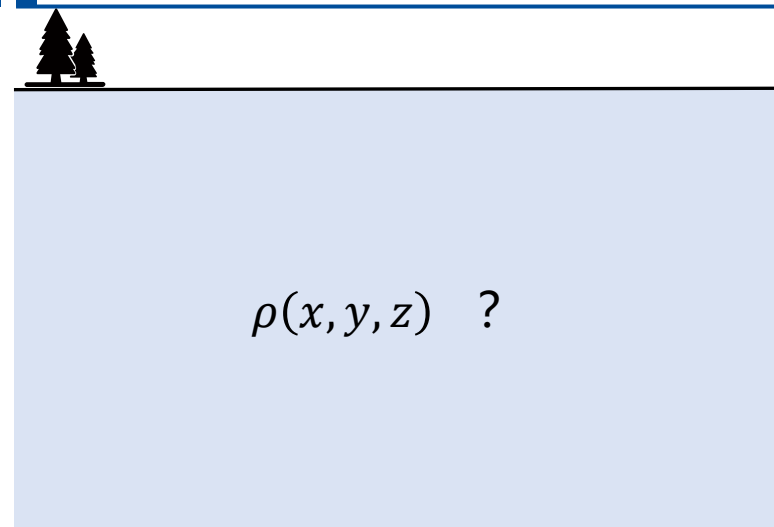
Minimum energy required for muon to penetrate volume:

$$E_{\text{min}} = aL_{\text{eff}} + b$$

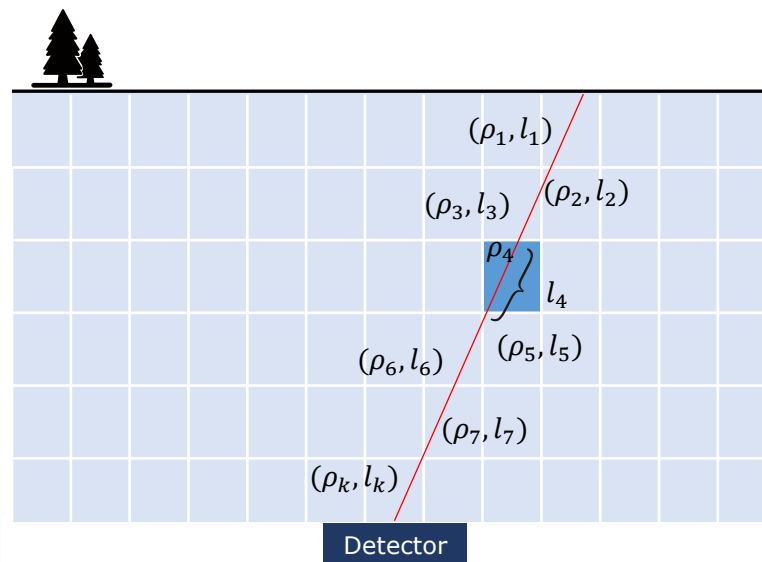


Data analysis and 3D inversion workflow of the muography approach

2.3 Forward and Inversion

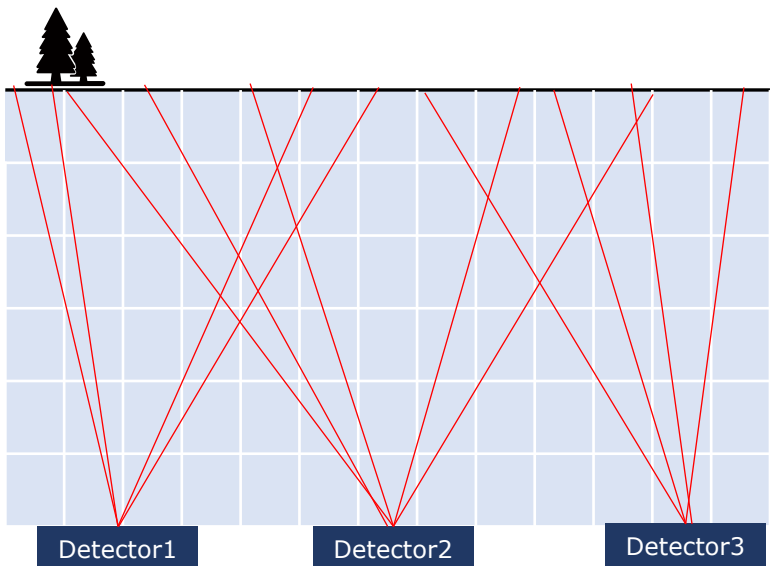


discretization

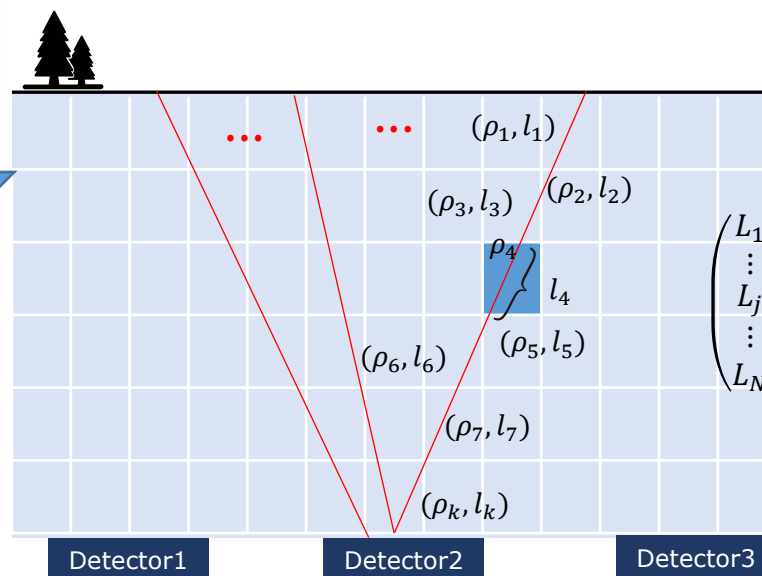


$$L_{\text{eff}} = \int \rho dl$$

$$L_{\text{eff}} = \rho_1 l_1 + \rho_2 l_2 + \dots + \rho_k l_k$$



$$L = G\rho$$



$$\begin{pmatrix} L_1 \\ \vdots \\ L_j \\ \vdots \\ L_N \end{pmatrix} = \begin{pmatrix} l_{11} & \dots & l_{1k} & \dots & l_{1M} \\ \vdots & & & & \vdots \\ l_{j1} & & \ddots & & l_{jM} \\ \vdots & & & & \vdots \\ l_{N1} & \dots & l_{Nk} & \dots & l_{NM} \end{pmatrix} \begin{pmatrix} \rho_1 \\ \vdots \\ \rho_j \\ \vdots \\ \rho_M \end{pmatrix}$$

- “fits the data”

$$\phi_{\text{misfit}}(\boldsymbol{\rho}) = \frac{1}{N} \sqrt{\sum_{i=1}^N \left(\frac{L_i^{\text{obs}} - L_i^{\text{pre}}}{\delta L_i} \right)^2}$$

$$\phi_{\text{misfit}} \sim 1$$

- “conforms the geology”

$$\phi_{\text{m}} = \alpha_s I(\boldsymbol{\rho} - \boldsymbol{\rho}_0) + (\alpha_x W_x + \alpha_y W_y + \alpha_z W_z) \boldsymbol{\rho}_2^2$$

where ρ_0 is a reference model; I is an identity matrix; $\alpha_s, \alpha_x, \alpha_y, \alpha_z$ are coefficients that affect the relative importance of different components and W_x, W_y, W_z are operators that calculate the continuity of density in the x -, y - and z -directions.

$$\phi_{\text{m}} \sim 0$$

- **Constraint condition:** $\rho_{\text{low}} < \rho < \rho_{\text{up}}$

Penalty function:

$$\phi_{\text{p}} = \sum_{j=1}^n \frac{[\max(0, \rho_j - \rho_{\text{up},j}) + \max(0, \rho_{\text{low},j} - \rho_j)]^2}{\rho_{\text{up},j} - \rho_{\text{low},j}}$$

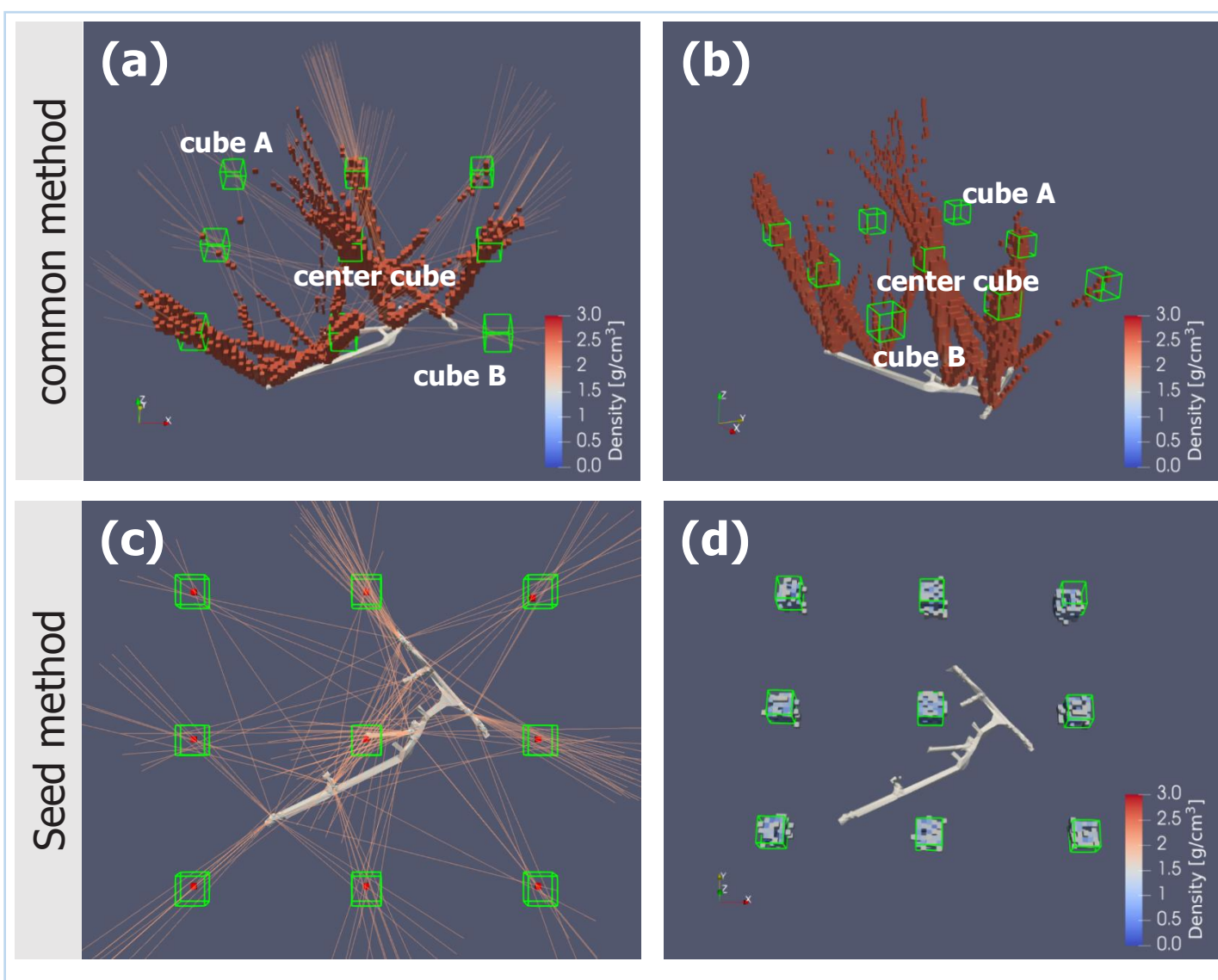
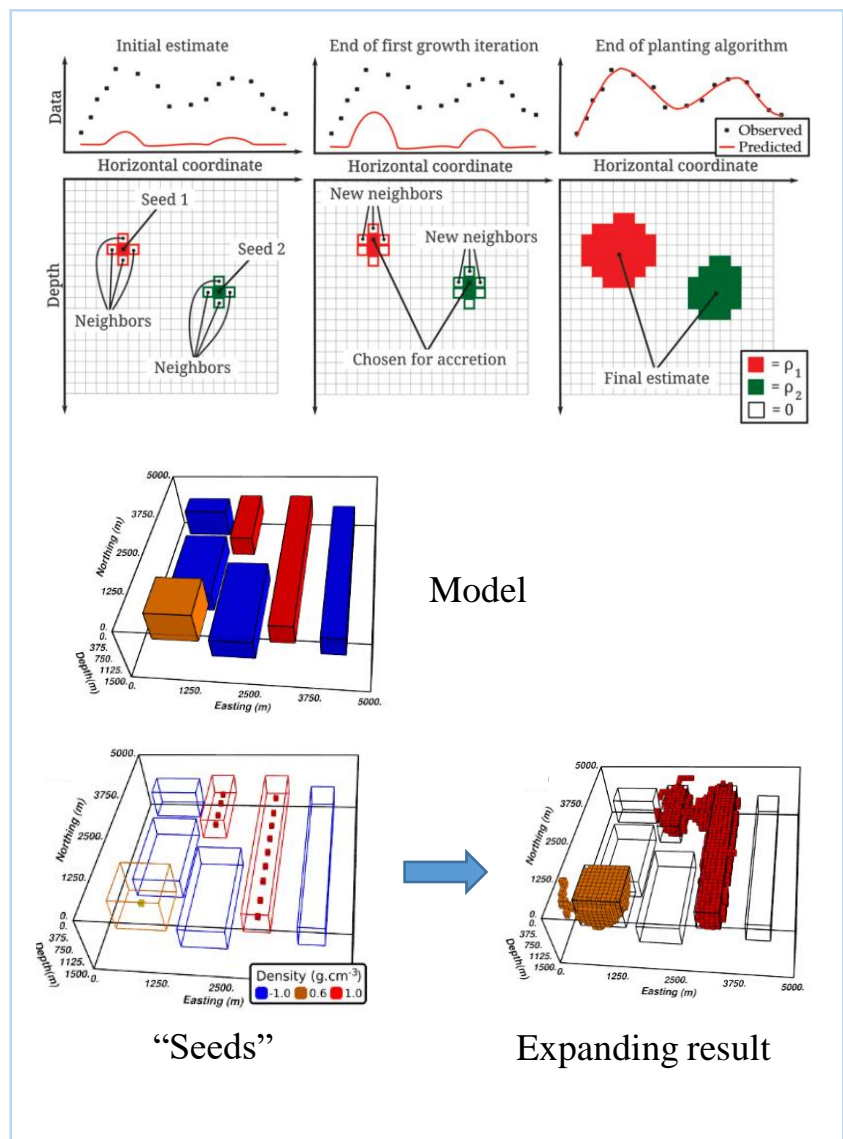
$$\phi(\boldsymbol{\rho}) = \phi_{\text{misfit}}(\boldsymbol{\rho}) + \beta \phi_{\text{m}}(\boldsymbol{\rho}) + \gamma \phi_{\text{p}}(\boldsymbol{\rho})$$

β : regularized factor
 γ : penalty coefficient

Minimize $\phi(\boldsymbol{\rho})$

Choose β so that $\phi_{\text{misfit}} \sim 1$

2.3 Inversion: “seed” method





Outline

01 / Introduction

02 / Muography System

03 / Cultural relics protection-Xi'an defensive walls

04 / Mineral Exploration-Zaozigou gold mine

05 / Summary and Prospect

3.1 Cultural relics protection-Xi'an defensive walls



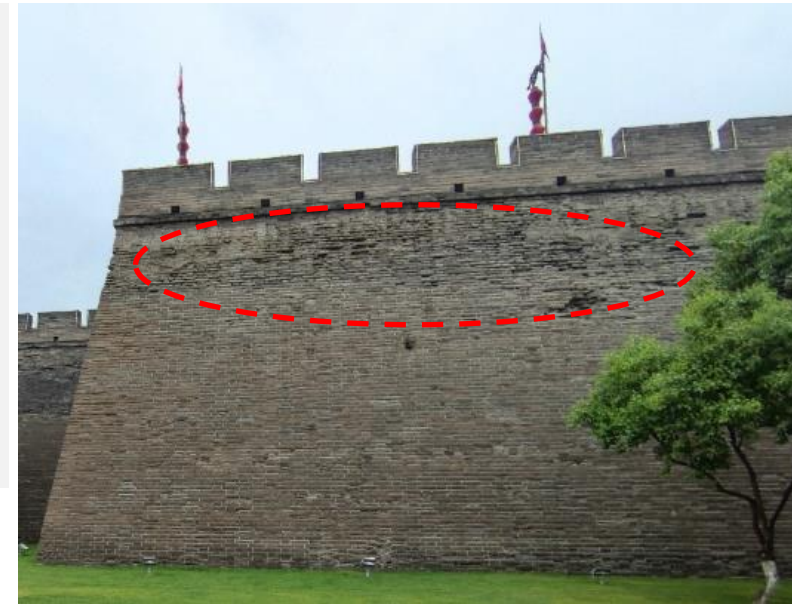
Xi'an

The capital of Shanxi Province, is located in northwest China.

Xi'an, identified by UNESCO as a "**World Historic City**" in 1981, is one of the important birthplaces of Chinese civilization and the Chinese nation, the starting point of the overland Silk Road, and the ancient capital of the Thirteen Dynasties.

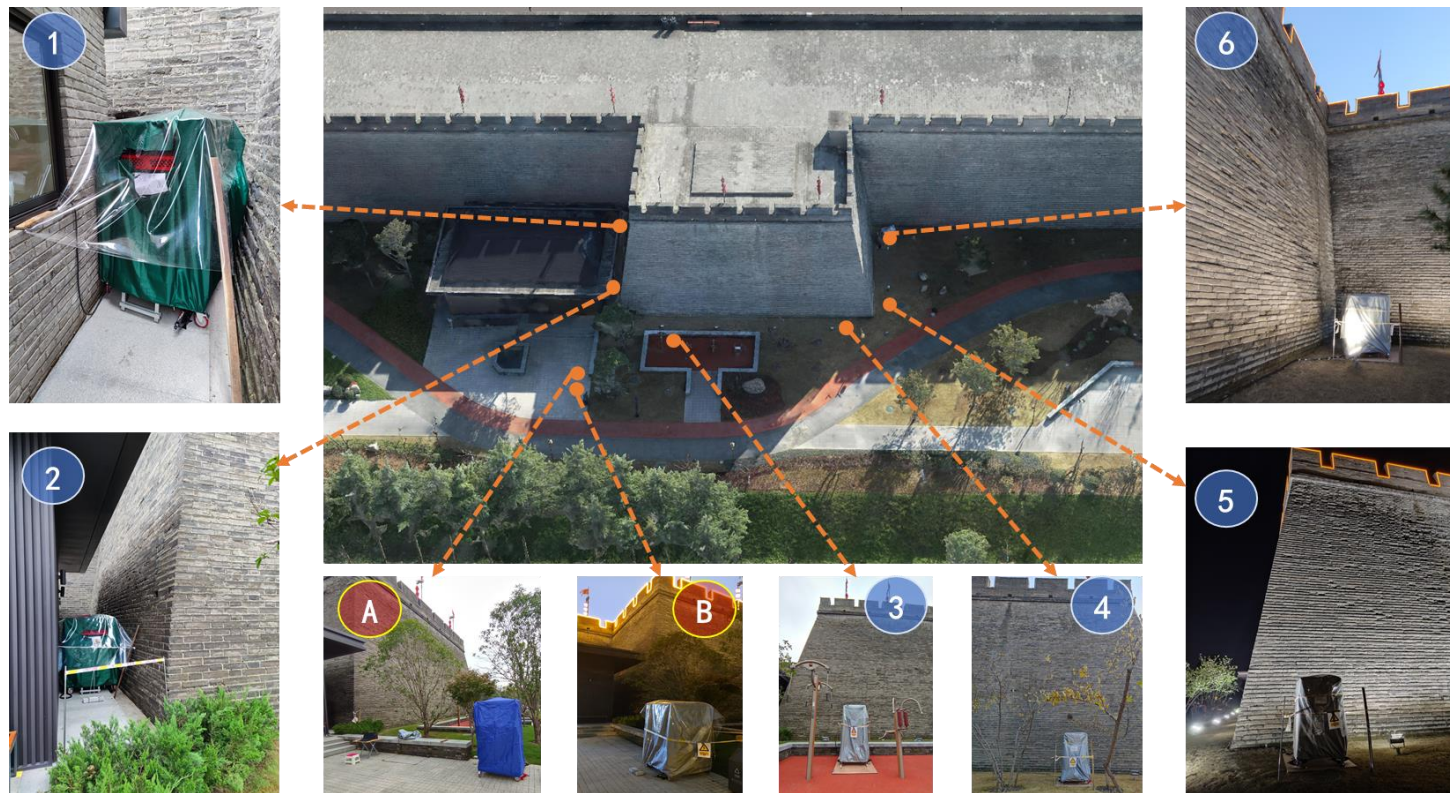
Problems faced by conservation monitoring of large cultural properties:

- ❑ Cultural relics can't move, can't destroy
- ❑ Damage too deep to detect
- ❑ Poor precision of detection results



3.2 Rampart No.58

Target region: Rampart No.58

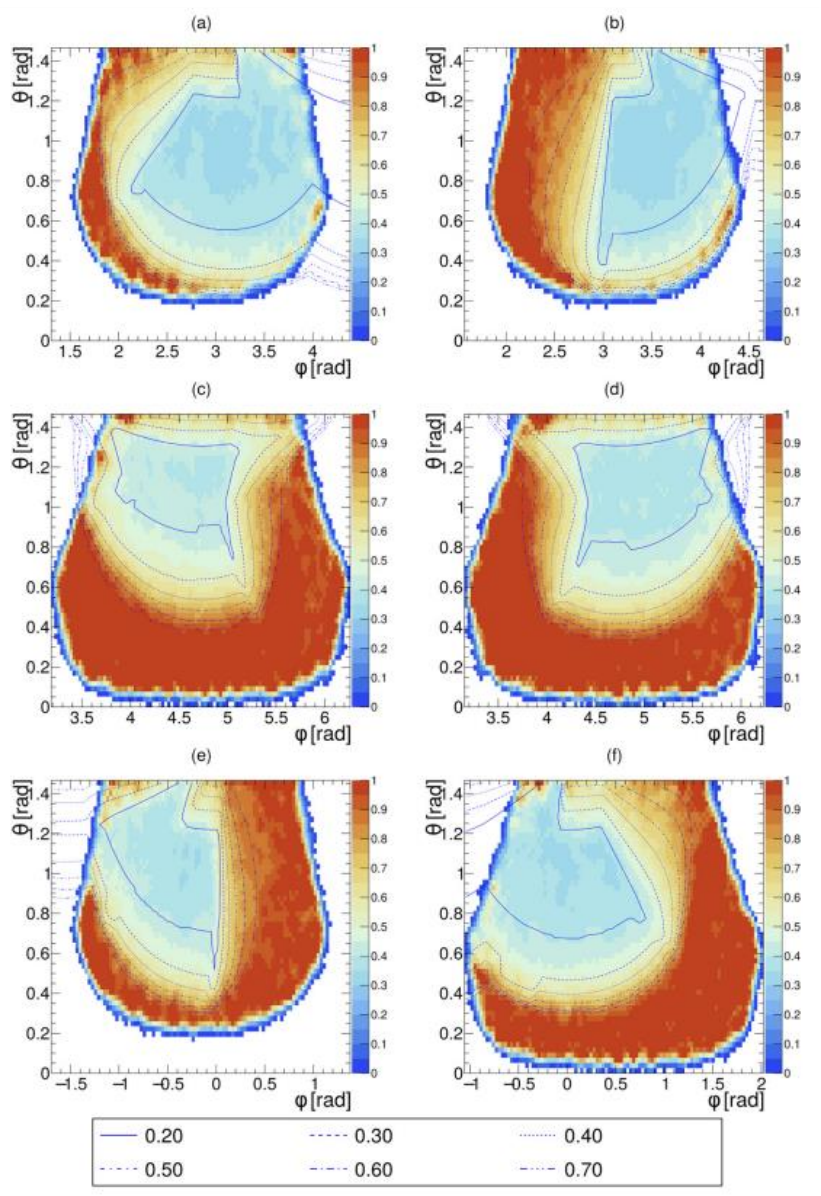


Layout of measurement location used in the on-site survey: (1-6) detector locations, (A and B) open-sky locations

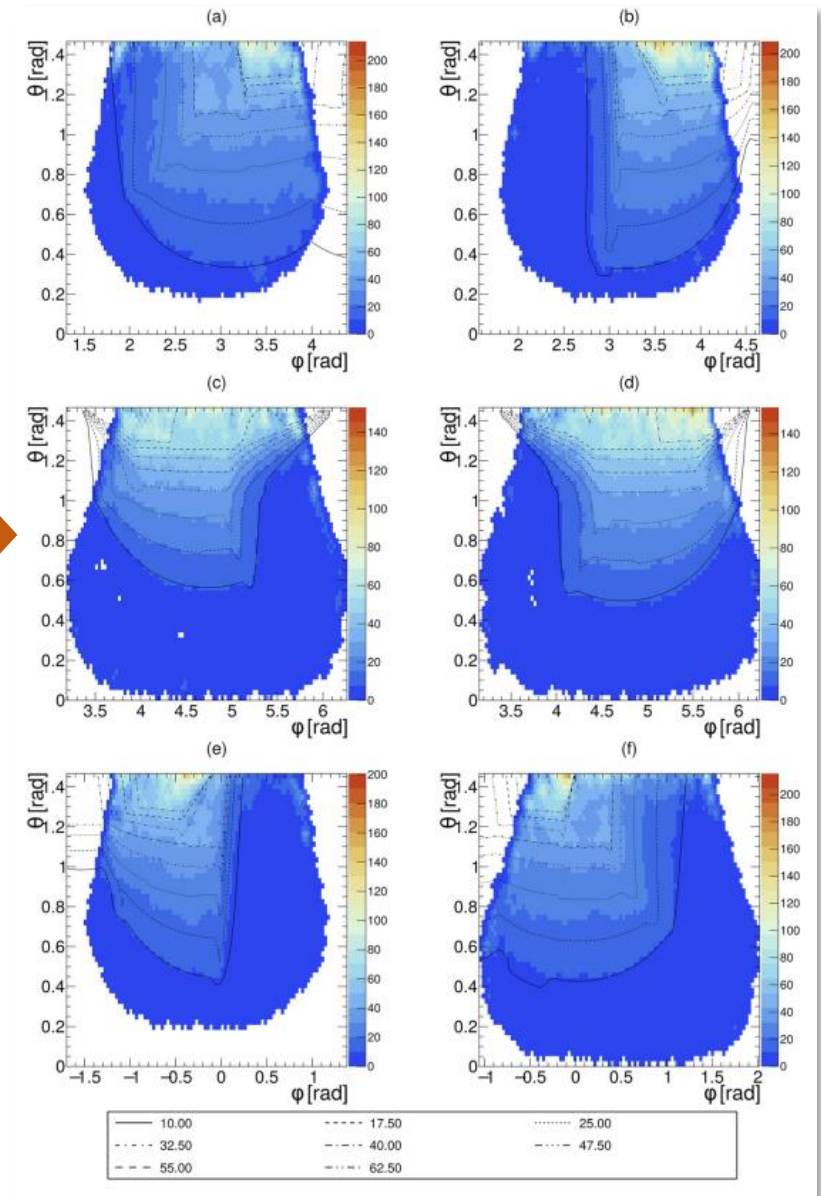
Experimental information

Location	Azimuth angle(°)	Zenith angle(°)	Duration (days)	Total count	Count rate(/h)
1	163.10	69.70	7.8	664708	4455
2	178.20	69.57	9.7	1168963	5769
3	270.66	60.55	13.9	1772770	8608
4	268.74	58.94	9.0	2040626	9287
5	-9.10	69.96	8.2	1171220	6738
6	27.60	59.47	8.8	1761860	8698
A	25.00	60.00	3.0	1175291	15366
B	90.00	70.00	2.8	911615	10752

3.3 Data analysis



Comparison of measured and predicted survival rate at six measurement points

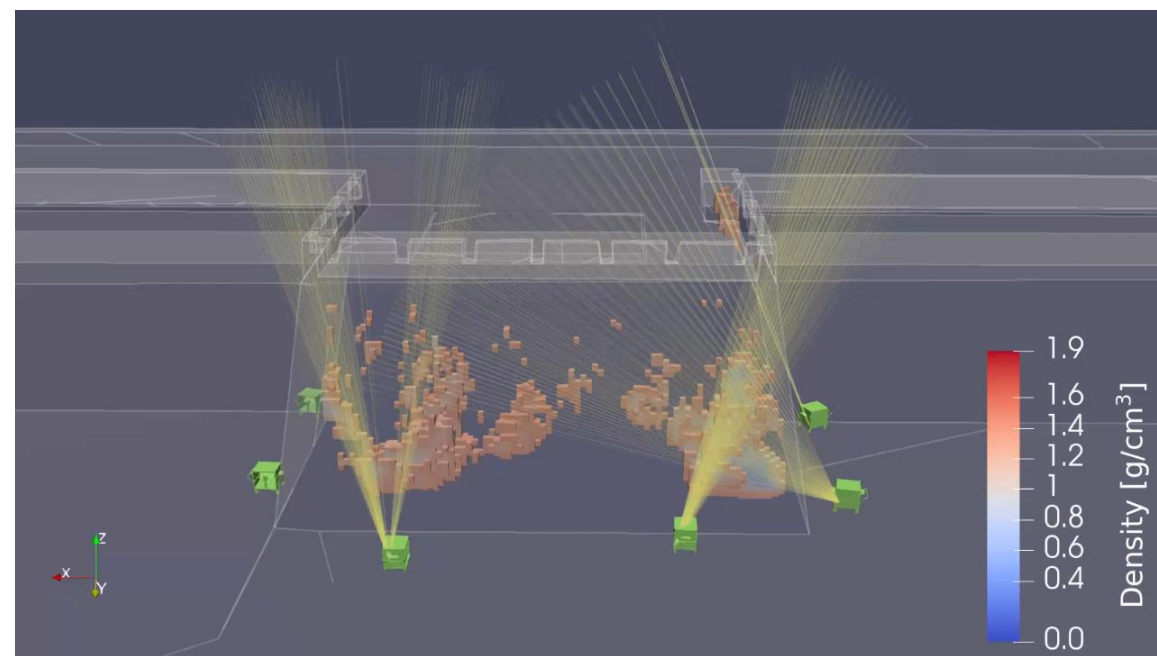
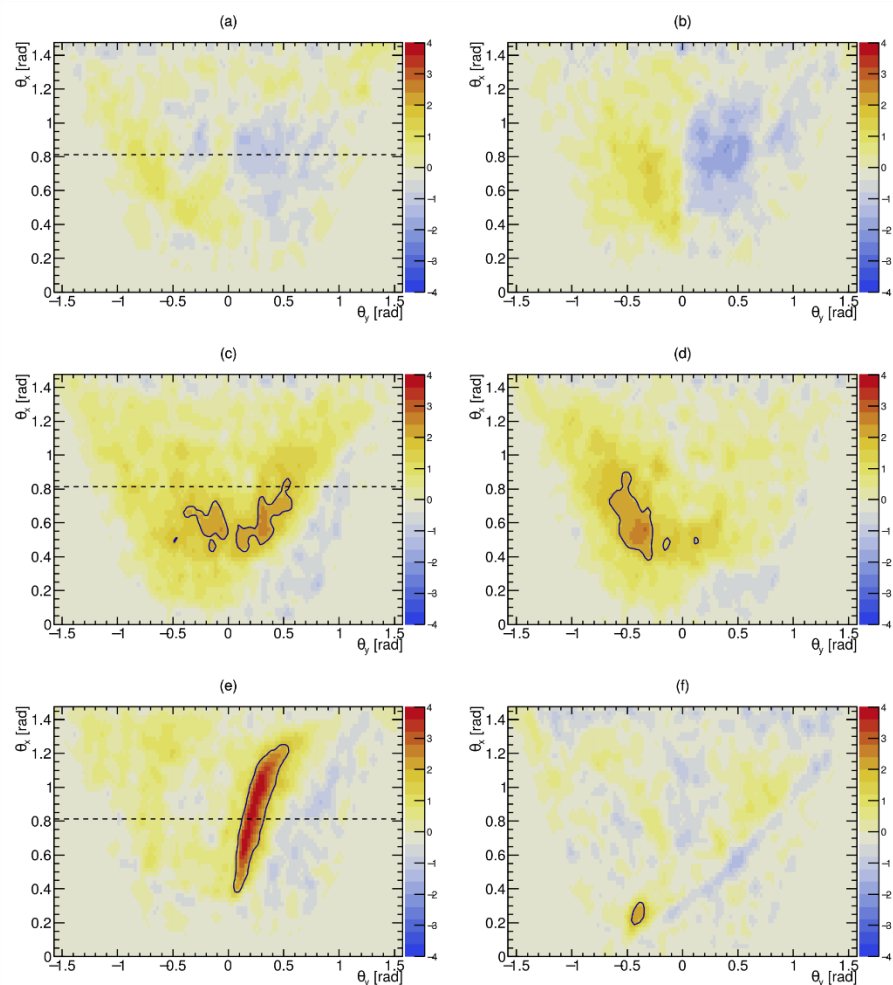


Comparison of measured and predicted effective lengths at six measurement points

3.4 Imaging results

$$\text{Significance: } \text{Sig}(\theta_x, \theta_y) = \frac{R_{\text{meas}}(\theta_x, \theta_y) - R_{\text{pre}}(\theta_x, \theta_y)}{\sigma_{\text{meas}}(\theta_x, \theta_y)}$$

- Sig: Characterizing the degree of significance of the difference between the measured and predicted values, the larger the absolute value of Sig indicates that the more significant the difference between the measured and forward predicted results in this direction, the higher the confidence level of the existence of density anomalies.





Outline

01 / Introduction

02 / Muography System

03 / Cultural relics protection-Xi'an defensive walls

04 / Mineral Exploration-Zaozigou gold mine

05 / Summary and Prospect

4.1 Mineral Exploration-Zaozigou gold mine



Hezuo

The capital of Gannan Tibetan Autonomous Prefecture in Gansu Province is located in the southwestern part of Gansu Province. The climate belongs to the alpine and humid type, with an average altitude of 3000 m.

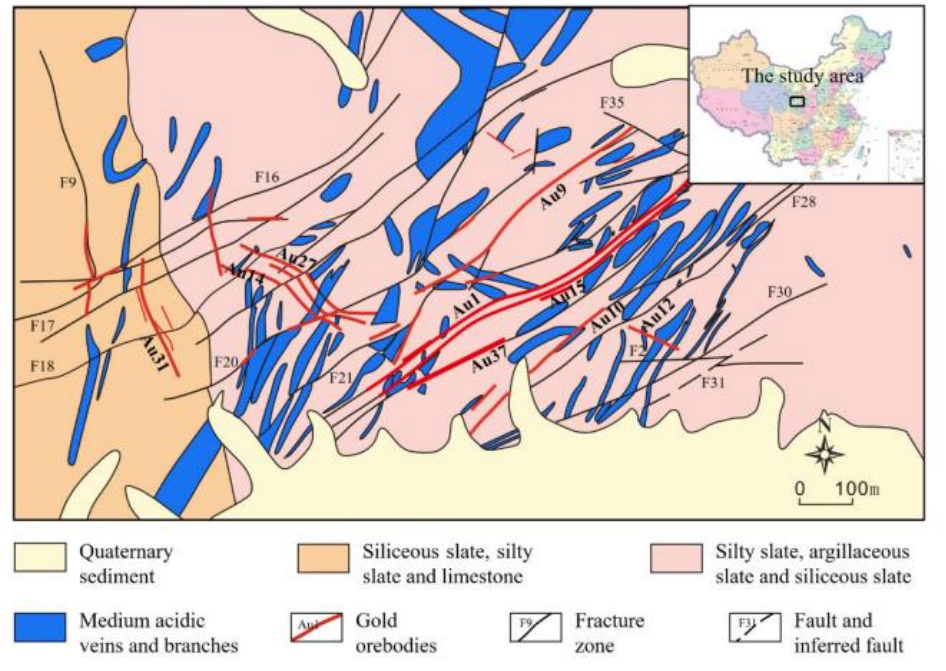
Problems faced in the mineral exploration :

- ❑ **Electrical and magnetic methods are limited in scale and susceptible to interference.**
- ❑ **Gravity and seismic methods have a large detection range but limited precision.**
- ❑ **High cost of commonly used drilling methods.**



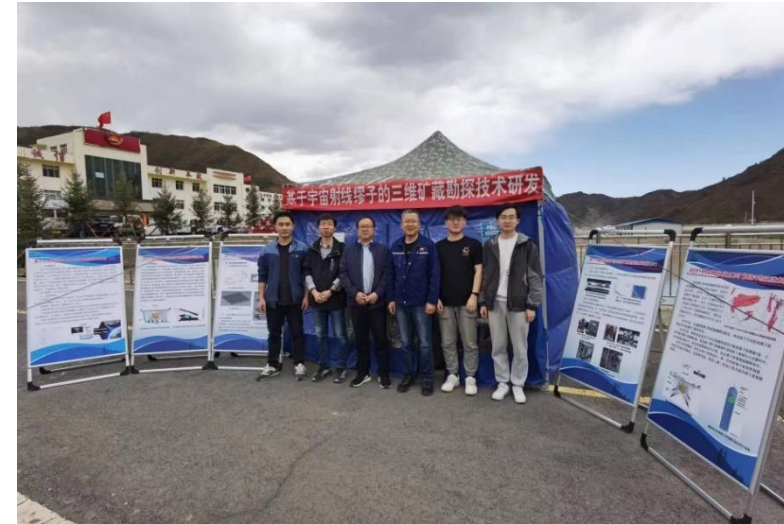
4.2 Zaozigou gold mine experiment

The geological map of the Zaozigou deposit

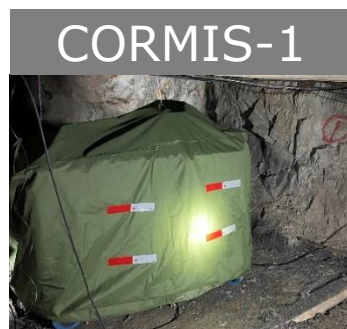
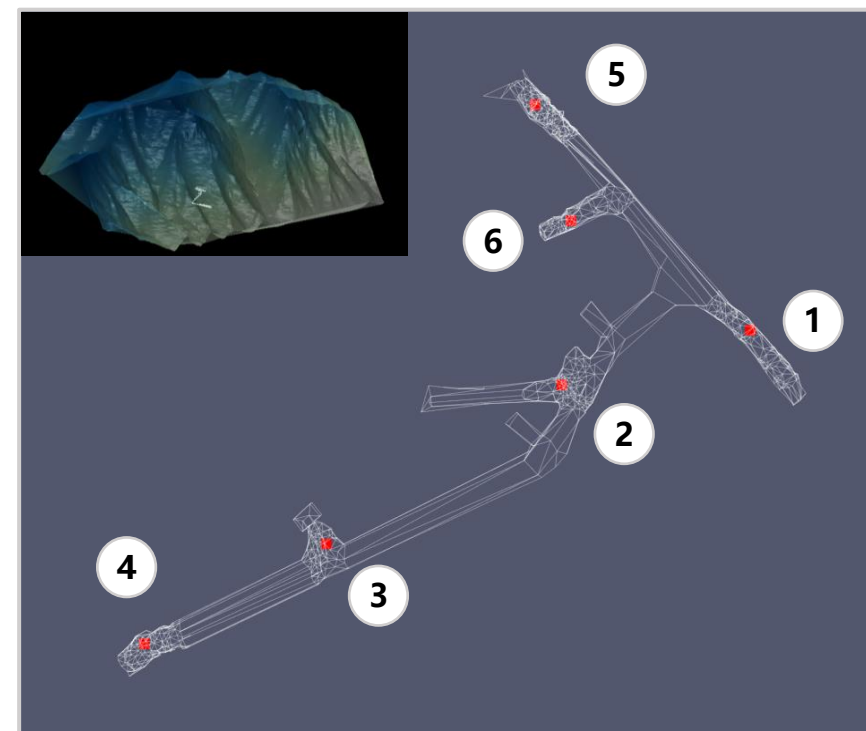
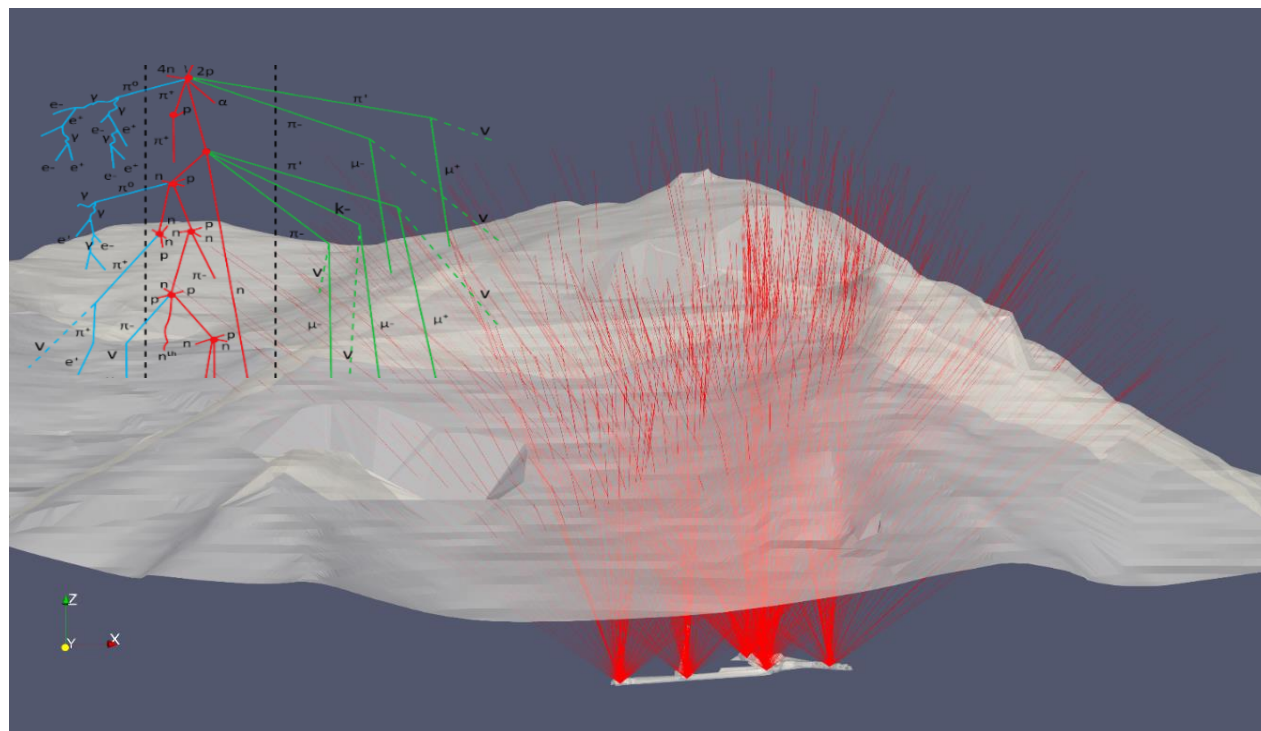


- ❑ Magmatic intrusion and faulting cause diverse attitudes of rocks, making geophysical identification and investigation difficult.
- ❑ Their average densities are 2.60, 2.64 and 2.63 g/cm³, respectively, when their gold grades are lower than 1.5. For higher grade areas, their average densities are greater than 2.7 g/cm³, less than 0.1 g/cm³ higher than surroundings.

On-site open-sky experiment



4.2 Zaozigou gold mine experiment



Experimental position in the tunnel

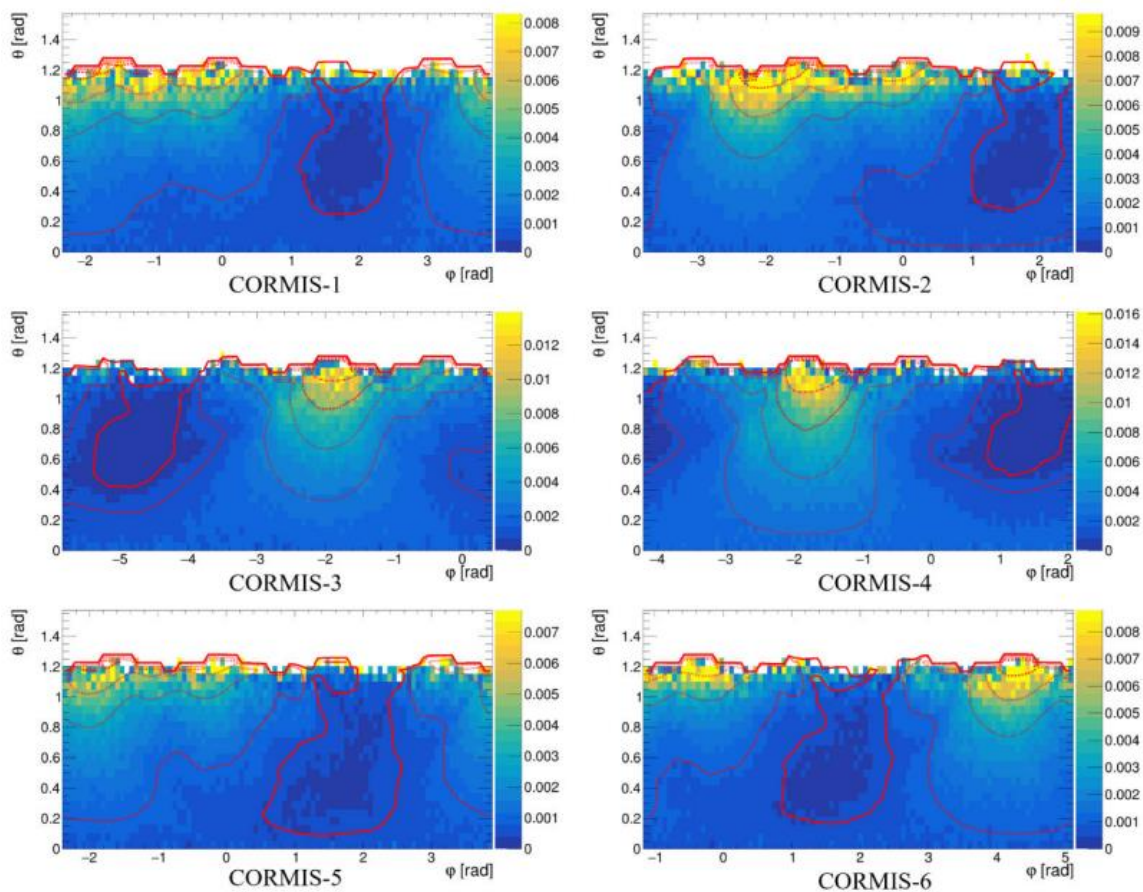
4.2 Zaozigou gold mine experiment

Experimental information

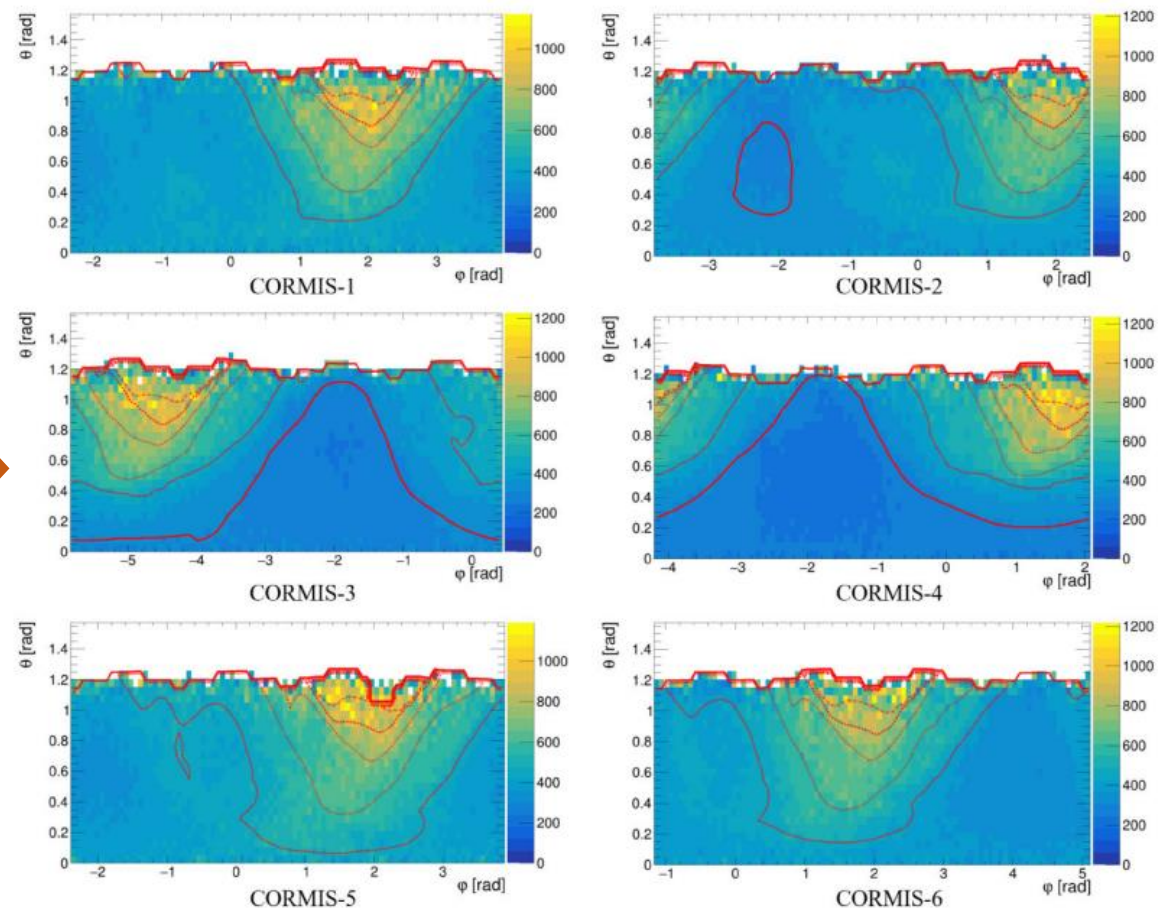
Detector	Measurement location	Total counts	Effective measurement duration(day)	Count rate(per day)
CORMIS-1	Free sky	4345193	1.68	2587529.64
	In tunnel	331521	119.63	277.13
CORMIS-2	Free sky	6386753	2.55	2507761.93
	In tunnel	489450	149.66	3270.42
CORMIS-3	Free sky	5074 734	2.01	2529243.56
	In tunnel	639 393	144.18	4434.62
CORMIS-4	Free sky	4297 730	1.63	2629809.71
	In tunnel	947 499	153.78	6161.23
CORMIS-5	Free sky	6895 140	2.76	2495309.19
	In tunnel	291 823	123.78	2357.62
CORMIS-6	Free sky	4110 971	1.63	2527631.93
	In tunnel	462 379	167.38	2762.44

4.3 Data analysis

Comparison of measured and predicted **survival rate** at six measurement points

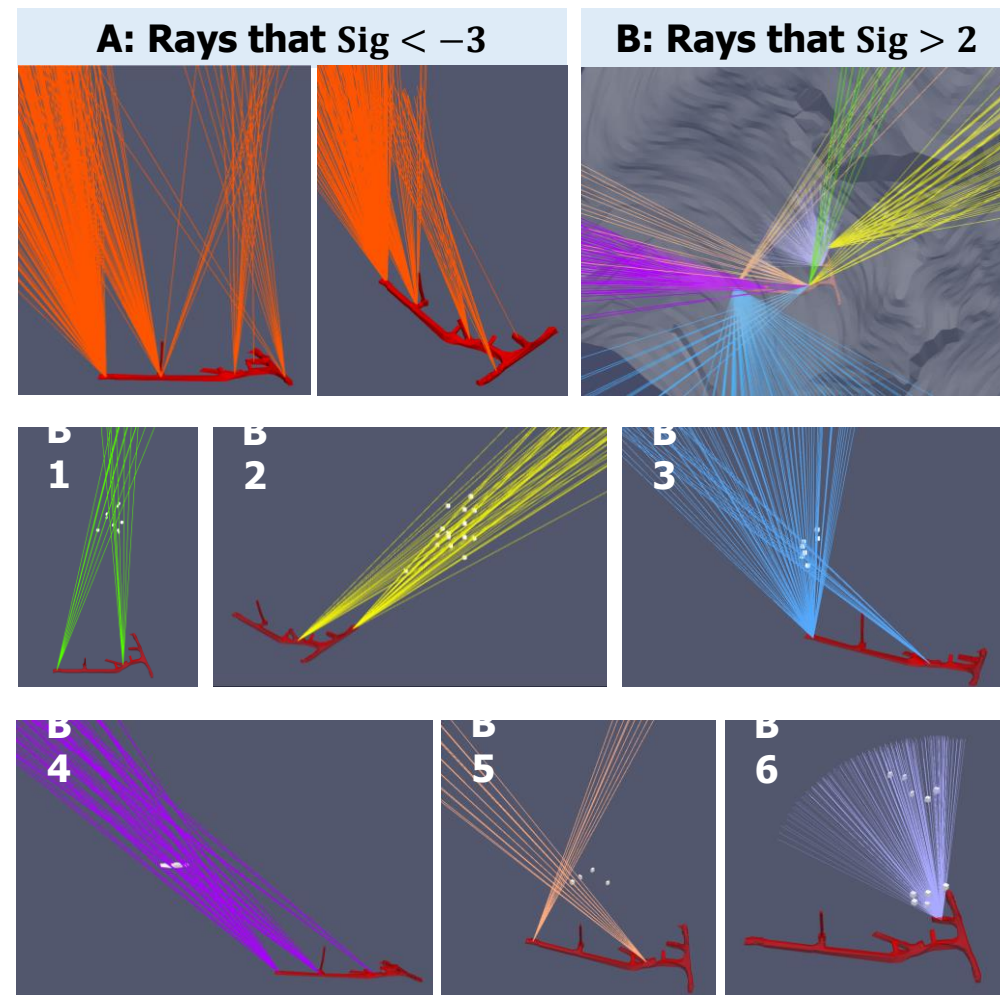
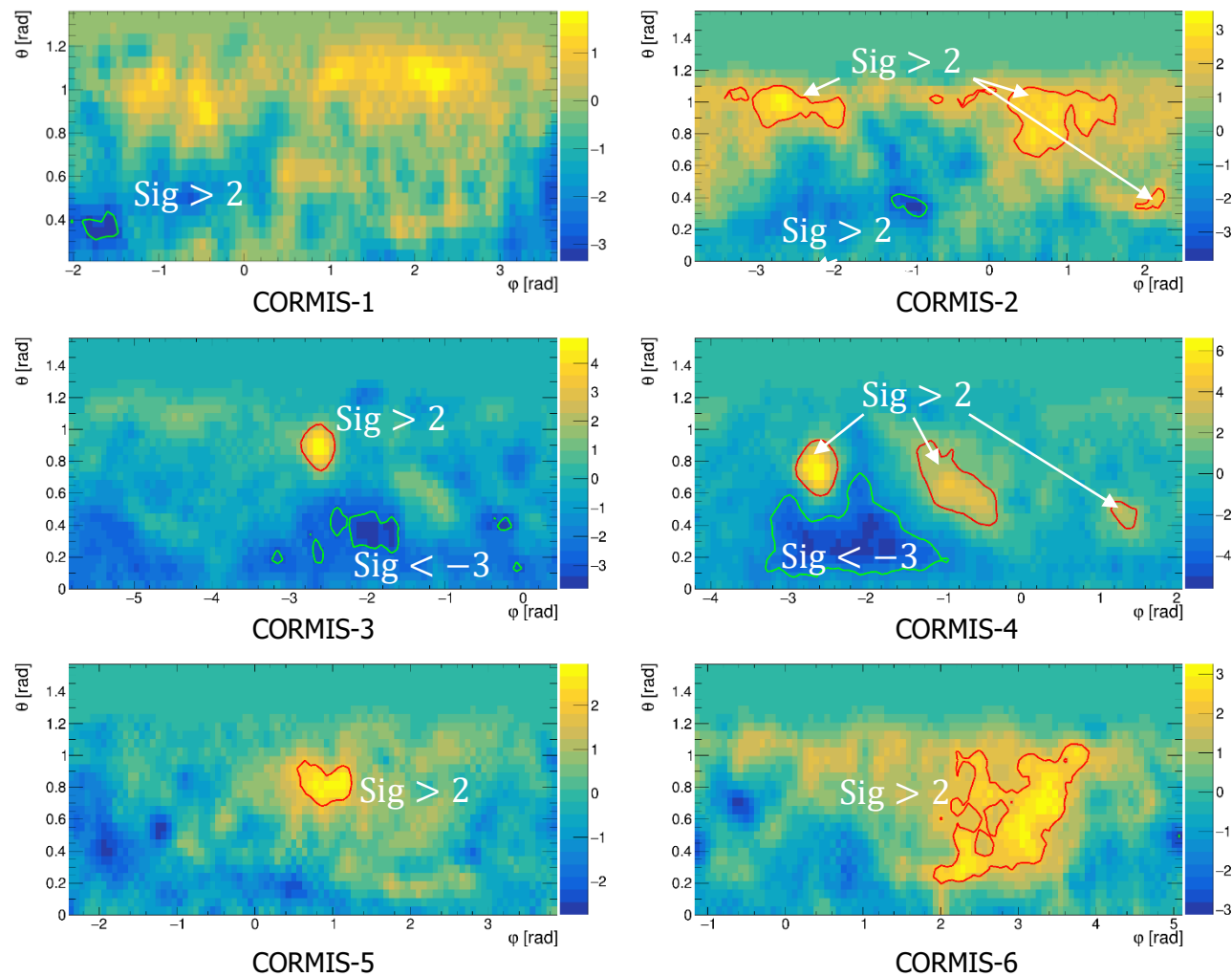


Comparison of measured and predicted **effective length** at six measurement points



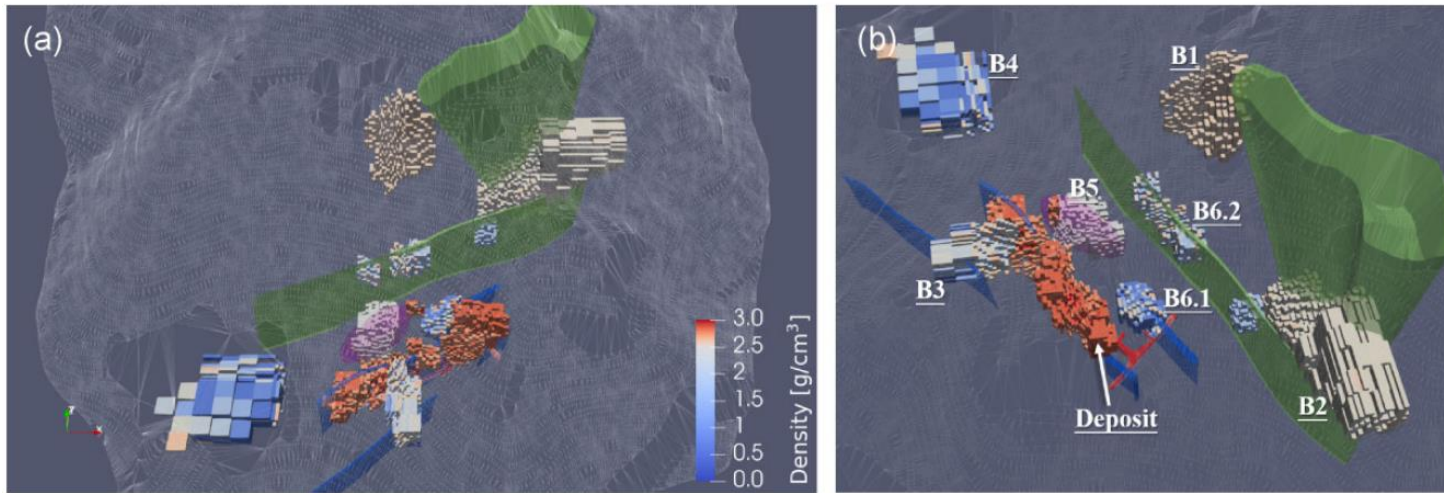
4.5 Inversion

$$Sig(\theta_x, \theta_y) = \frac{R_{meas}(\theta_x, \theta_y) - R_{pre}(\theta_x, \theta_y)}{\sigma_{meas}(\theta_x, \theta_y)}$$



Select initial “seeds” (white grid) in the overlapping areas

4.6 Imaging results



Reconstructed anomalies in region B1-B6 with the seed algorithm. Green surfaces: mined ore body model. Blue surface: the ore body models with uncertain mining status. The surface in B5: the model of the limonitic siliceous slate.

- Discovered four mined-out areas; half of them are confirmed by the documentation.
- Reconstructed the limonitic siliceous slate whose density are slightly different from the bulk density.

Region	Density(compared to the bulk density)	Size(m^3)	Classification
Above tunnel	Higher	34333	Gold ore body
B1	Slightly lower	6516	Scarps
B2	Slightly lower	42920	Mined-out area (uncompacted backfill)
B3	Much lower	8000	Mined-out area
B4	Much lower	25648	Stope
B5	Slightly lower	3672	Limonitic siliceous slate structure
B6.1	Much lower	4860	Mined-out area
B6.2	Much lower	9334	Mined-out area



Outline

01 / Muography

02 / Muography System

03 / Cultural relics protection-Xi'an defensive walls

04 / Mineral Exploration-Zaozigou gold mine

05 / Summary and Prospect

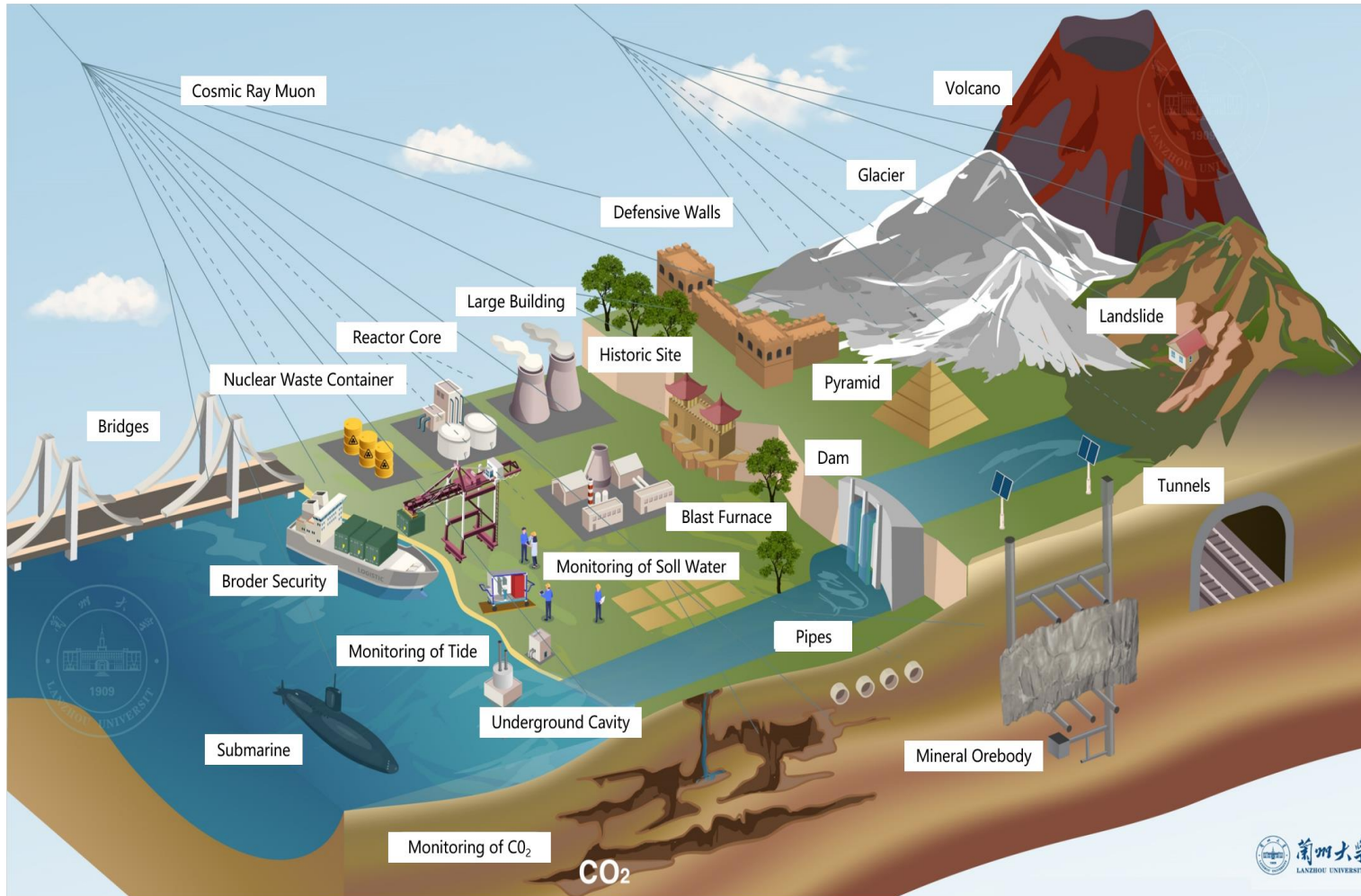
Achievement

- ✓ Successful implemented domestic's first application of Muography in cultural relics conservation
- ✓ Successfully implemented Asia's first application of Muography in mineral exploration

Importance

The successful implementation of the experiment demonstrates that Muography has great advantages in the field of cultural relics conservation and mineral deposit exploration.

- ❑ A complete data analysis process
- ❑ Application to low-density-contrast ore body exploration
- ❑ Analysis of altitudinal impacts on muography, and giving a simplified method to eliminate impact
- ❑ Development of precise and efficient reconstruction algorithms: **“seed” algorithm**



Application scenarios of Muography

1. Detector

- Miniaturization: for scenes where space is at a premium
- Large size: improved imaging efficiency
- Low cost, high reliability

2. Software platforms and algorithms

Lowering the threshold of use for non-professionals by integrating simulation, data analysis, forward and backward modelling into a single platform; optimizing algorithms to obtain reliable imaging in valid event situations.

3. On-site implementation

There is a lack of processes to produce and optimize the implementation of scenarios in the field and to assess the feasibility of the scenarios. There are many more existing scenarios to be developed.



兰州大学

LANZHOU UNIVERSITY

THANKS!